Volume 24
Number 14
21 July 2024
Pages 3317–3570

Lab on a Chip

Devices and applications at the micro- and nanoscale

rsc.li/loc

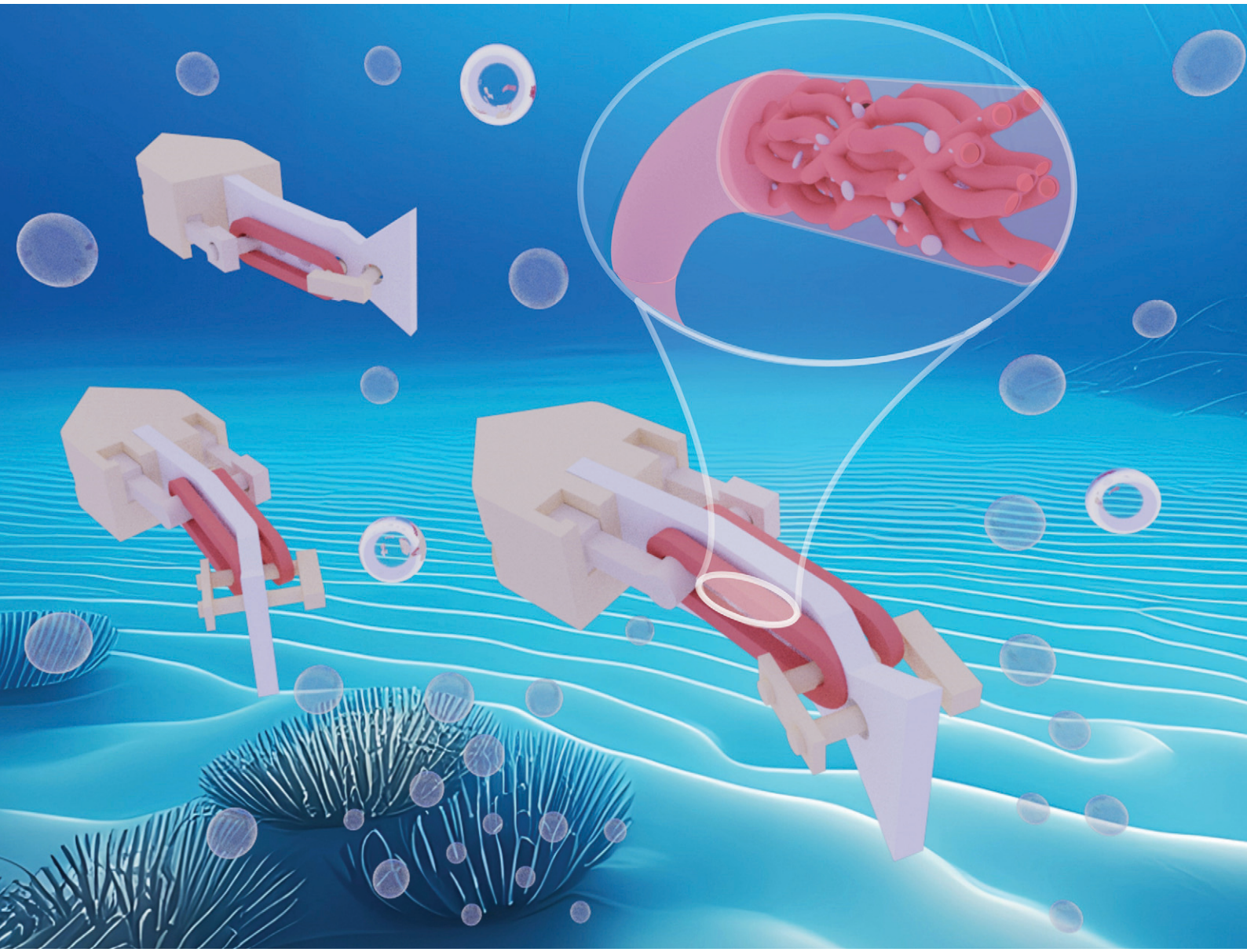

ISSN 1473-0197

ROYAL SOCIETY OF CHEMISTRY

PAPER
Shoji Takeuchi *et al.*
Human induced pluripotent stem cell-derived cardiac muscle rings for biohybrid self-beating actuator

Lab on a Chip

PAPER

View Article Online
View Journal | View Issue

Check for updates

Cite this: *Lab Chip*, 2024, **24**, 3377

Human induced pluripotent stem cell-derived cardiac muscle rings for biohybrid self-beating actuator†

Tomohiro Morita,[a] Minghao Nie [a] and Shoji Takeuchi *[abc]

Cardiac muscle, a subtype of striated muscle composing our heart, has garnered attention as a source of autonomously driven actuators due to its inherent capability for spontaneous contraction. However, conventional cardiac biohybrid robots have utilized planar (2D) cardiac tissue consisting of a thin monolayer of cardiac myotubes with a thickness of 3–5 μm, which can generate a limited contractile force per unit footprint. In this study, 3D cardiac muscle rings were proposed as robotic actuator units. These units not only exhibit higher contractile force per unit footprint compared to their 2D counterparts due to their increased height, but they can also be integrated into desired 3D configurations. We fabricated cardiac muscle rings from human induced pluripotent stem cell-derived cardiomyocytes (hiPSC-CMs), evaluated their driving characteristics, and verified the actuation effects by integrating them with artificial components. After the 10th day from culture, the cardiac muscle rings exhibited rhythmic spontaneous contraction and increased contractile force in response to stretching stimuli. Furthermore, after constructing a centimeter-sized biohybrid self-beating actuator with an antagonistic pair structure of cardiac muscle rings, the periodic antagonistic beating motion at its tail portion was confirmed. We believe that 3D cardiac muscle rings, possessing high contractile force and capable of being positioned within limited 3D space, can be used as potent biohybrid robotic actuators.

Received 29th March 2024,
Accepted 28th May 2024

DOI: 10.1039/d4lc00276h

rsc.li/loc

Open Access Article. Published on 15 June 2024. Downloaded on 8/2/2025 4:02:20 PM.
This article is licensed under a Creative Commons Attribution-NonCommercial 3.0 Unported Licence.

Tribute to George Whitesides

It is with great respect and admiration that I contribute to this special collection celebrating the 85th birthday of George Whitesides. My journey in microfluidics and lab-on-a-chip technology has been profoundly influenced by his pioneering work, inspiring generations of scientists and countless advancements.

I had the privilege of being a Visiting Scholar in George's group from 2004 to 2005. Despite the short duration, the research environment was remarkable. As a budding researcher, I bombarded him with questions, and each response was eye-opening. The interdisciplinary nature of his lab was highly stimulating, and I remain in contact with many members who continue to inspire me. I vividly remember George drawing three overlapping circles labelled Bio, Materials, and Physics, encompassed within a larger circle labelled Chemistry, emphasizing that everything is Chemistry. This holistic view left a lasting impression on me, and I aspire to develop a similarly comprehensive approach in my own research.

I also recall my farewell party when George praised my research on biohybrid insect robots. His encouragement motivated me to continue this research, forming the foundation of my current studies. George's contributions extend beyond his groundbreaking scientific achievements. His mentorship and commitment to nurturing young scientists have created a legacy that will endure. I am deeply grateful for the opportunities and guidance I received under his mentorship and am honoured to be part of this tribute.

Introduction

Biohybrid robots are robotic systems that integrate biological actuators driven by living cells with artificial components, enabling the emulation of adaptive movements and response outputs of living organisms to environmental stimuli.[1] Amongst the biological actuators, muscles are popular for their high output efficiency, with striated muscles such as skeletal and cardiac muscles.[2] Especially, immature

[a] *Department of Mechano-Informatics, Graduate School of Information Science and Technology, The University of Tokyo, 113-8656, Japan.*
E-mail: takeuchi@hybrid.t.u-tokyo.ac.jp
[b] *Institude of Industrial Science (IIS), The University of Tokyo, 153-8505, Japan*
[c] *International Research Center for Neurointelligence (WPI-IRCN), the University of Tokyo Institutes for Advanced Study (UTIAS), 113-0033, Japan*
† Electronic supplementary information (ESI) available. See DOI: https://doi.org/10.1039/d4lc00276h

Open Access Article. Published on 15 June 2024. Downloaded on 8/2/2025 4:02:20 PM.
This article is licensed under a Creative Commons Attribution-NonCommercial 3.0 Unported Licence.

cardiomyocytes with artificially modified expression profiles and/or artificially engineered cardiac muscle tissues are known to exhibit spontaneous contraction, having been garnering attention as potential sources of actuation.

Conventional biohybrid actuators powered by cardiac muscles have been composed of planar cardiac muscle tissues (2D cardiac muscle tissues) formed on a planar substrate. The self-contraction of the cardiac muscle tissues directly transmits the traction force to the substrates, allowing the actuator to walk on a dish or swim in a culture medium by deforming the substrates.[3–10] To achieve further deformation of substrates with the same lengths and widths, it is

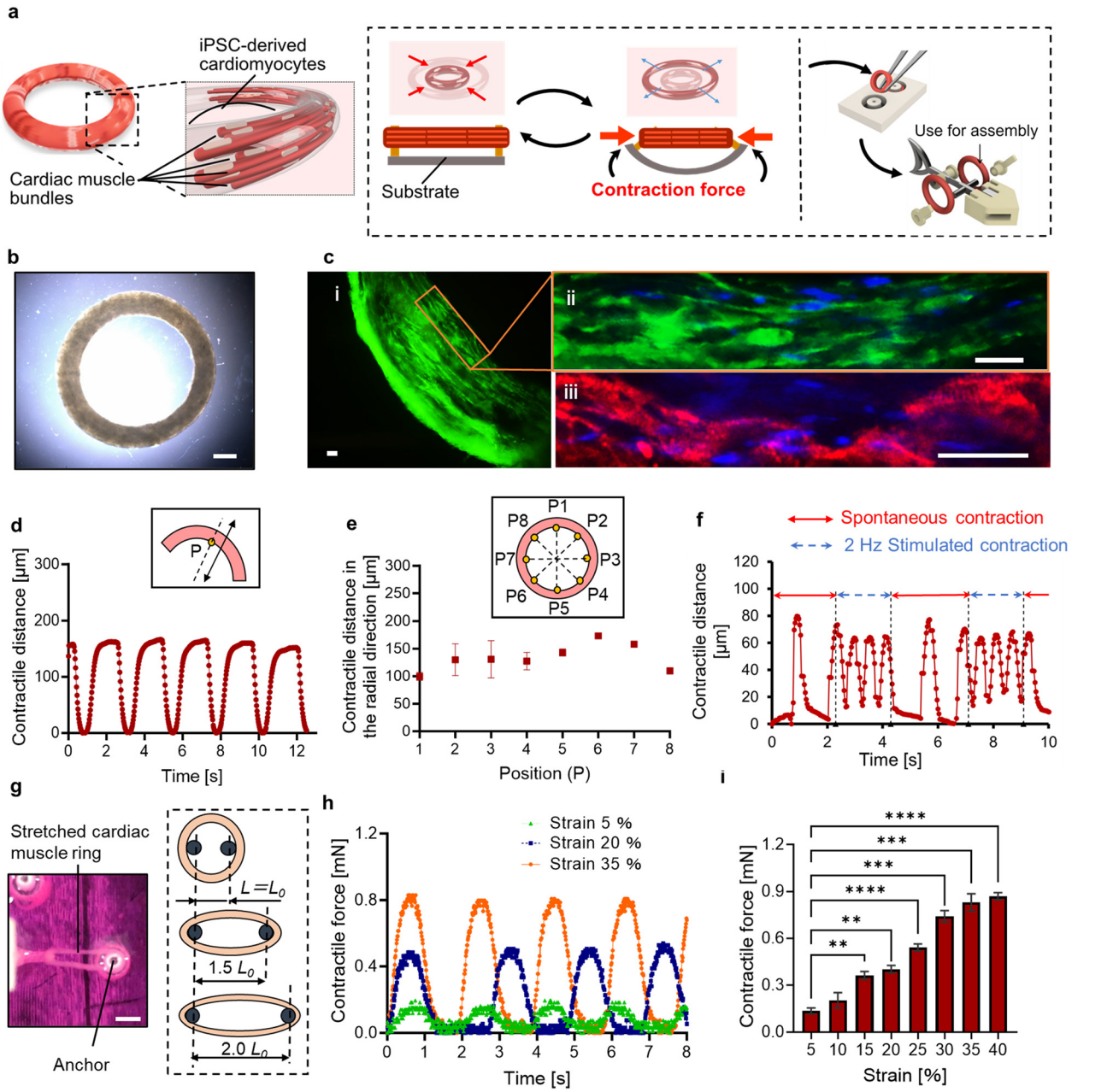

Fig. 1 Functional and morphological evaluation of the cardiac muscle ring. (a) Conceptual images of the cardiac muscle ring and its spontaneous contraction. (b) A cardiac muscle ring removed from the PDMS substrate. (c) Immunostaining image of a cardiac muscle ring ((i) a part of a cardiac ring (stained by F-actin), (ii) enlarged view (stained by F-actin and Nuclei), (iii) enlarged view (stained by α-actinin and nuclei)). Green; F-actin. Red; α-actinin. Blue; nuclei. (d) Temporal distance of the tracking point P placed on a cardiac muscle ring with its spontaneous contraction. The inset shows the conceptual image of the tracking point P and its moving direction. (e) Contractile displacement in the radial direction of the eight tracking points placed on a cardiac muscle ring. Inset shows the conceptual image of eight evenly spaced reference points placed on a cardiac ring. (f) Temporal contractile distance of a cardiac muscle ring when the electric field is intermittently applied. (g) Images for measuring contractile forces of the cardiac muscle rings. One of the ends of a cardiac muscle ring is connected to the force sensor. The external stretching stimulus is applied to a cardiac muscle ring by varying the distance between the anchors. (h) Temporal changes of the contractile force induced by spontaneous contraction of a cardiac muscle ring. (i) The relationship between the applied strain and the measured contractile force. Bars represent the mean ± SEM. $^{**}p < 0.005$, $^{***}p < 0.0005$, $^{****}p < 0.0001$, Tukey–Kramer test ($n = 4$). Scale bars; a: 500 μm. b: 100 μm. c: 20 μm.

This journal is © The Royal Society of Chemistry 2024

Open Access Article. Published on 15 June 2024. Downloaded on 8/2/2025 4:02:20 PM.
This article is licensed under a Creative Commons Attribution-NonCommercial 3.0 Unported Licence.

ideal to increase the contractile force per unit footprint of the cardiac muscle tissues. However, the thickness of a monolayer of 2D cardiac muscle tissue is limited to 3–5 μm, necessitating the stacking of multiple layers of constructed 2D cardiac muscle tissue to increase its thickness. Furthermore, for 2D cardiac muscle tissues, complex surface modifications on the substrates are required to orient cardiac cells to exert force in a desired direction.[4,5,8,11–13]

In this study, 3D cardiac muscle rings derived from human induced pluripotent stem cells (hiPSCs) were proposed as robotic actuator units. 3D cardiac muscle tissues can be constructed by injecting cell-suspended hydrogels within a mold, and the tissue dimensions can be adjusted according to the depths and widths of grooves formed in the mold. Therefore, it is easier to increase the thickness of 3D cardiac muscle tissues compared to their 2D counterparts, resulting in greater contractile forces per unit footprint. Furthermore, assembling the 3D cardiac muscle rings onto robots in a pick-and-place style allows for integration into 3D spatial configurations (Fig. 1a). Here, the properties of the cardiac muscle rings are evaluated, including contractile force, responsiveness to external stretching stimulus and electric stimulus. We then develop a centimeter-sized biohybrid self-beating actuator shaped resembling a fishtail, comprising an antagonistic pair of cardiac muscle rings. Finally, we demonstrate the actuation of the centimeter-scale tail structure with the power of the cardiac muscle rings and assess driving characteristics by observing its tail beating motion.

Results

Functional and morphological evaluation of 3D cardiac muscle tissues

The gelation and culture within the substrate made from poly-dimethylsiloxane (PDMS) resulted in the formation of cell-suspended hydrogels molded into a ring shape. On the 14th day of culture, a cardiac muscle ring was extracted from a flexible substrate made from polydimethylsiloxane (PDMS) (Fig. 1b). To facilitate easy extraction of the tissue, 0.5 wt% phosphorylcholine (MPC) polymer was coated onto the PDMS substrate prior to seeding cell suspensions and was found to be effective in preventing the adhesion of the 3D tissue to the surface of the PDMS substrate.

To evaluate the morphology of the cardiac muscle rings, immunohistochemical analysis was performed, revealing that human induced pluripotent stem cell-derived cardiomyocytes (hiPS-CMs) were elongated and formed muscle fibers. Furthermore, α-actinin, providing structural support for muscle contraction, was confirmed in the cardiac muscle ring (Fig. 1c). These results indicate that our cardiac muscle rings possess physiological-relevant tissue morphology.

A spontaneous and rhythmic contractile activity of a cardiac muscle ring was observed in a PDMS substrate on the 10th day from the start of culture. We then extracted a cardiac muscle ring and observed its contractile motion. The displacement on the reference point (point P) set on the circumference of the cardiac muscle ring was approximately 150 μm at intervals of 2.0 s (Fig. 1d). After reaching the maximum contraction, the cardiac muscle ring relaxed immediately and returned to nearly its original state. Furthermore, the diameter changes in the radial direction were observed at various locations of the tissue (Fig. 1e and Movie S1†). These results indicate that all cells within a cardiac muscle ring showed synchronized contractile activity due to the rapid cell-to-cell propagation of action potentials.[14] Additionally, for the evaluation of the response to the external stimuli, we applied an electric field to a cardiac muscle ring. When we applied an electrical signal of a pulse train at 2 Hz and 2.4 V mm^{-1}, the cardiac muscle ring exhibited stimuli-induced contraction (four times within two seconds) and returned to its spontaneous contraction (once within 1.3 seconds) when we stopped the stimuli (Fig. 1f). This result shows the motion controllability of the cardiac muscle ring in response to the electric field.

To investigate the responsiveness to the applied stretching stimulus, we attached the ends of the cardiac muscle ring to the force sensor (micro force type; THK Precision) and a 3D printed jig (Fig. S1†), respectively. In this experiment, we applied only stretching stimuli to the cardiac muscle ring and measured the exerted muscular force by its spontaneous contraction. Also, by varying the distance between the anchors, we applied external strain to the cardiac muscle ring (Fig. 1g). For example, when applying a 20% strain, we extended the distance between these anchors by 20% from the inner diameter of a cardiac muscle ring in its non-stretched state. As a result, we confirmed a direct correlation between the applied strain and the muscular contractile force, and the maximum value of 850 μN was obtained when over 35% of strain was applied (Fig. 1h and i). Furthermore, we compared the muscle rings cultured without and with (20%) the application of an initial strain. After 14 days of culture, we confirmed a 1.9-fold increase in contractile force of the cardiac muscle rings within antagonistic paired structure (Fig. S2.1†). These results suggest that stretching stimuli increased sarcomere length,[15] which enhanced the overlap between the actin and myosin filaments responsible for muscle contraction, leading to an increase in contractile force. Meanwhile, spontaneous contraction frequency did not change dramatically with increased strain (Fig. S2.2†). This result indicates that the intrinsic contraction frequency of cardiac cells is controlled by changes in the cell membrane potential and the dynamics of calcium ions,[16] which are not strongly affected by temporal external stretching stimuli.

Contractile forces of cardiac muscle rings with different dimensions

By altering the dimensions of the circular groove of the PDMS substrate, we captured fluorescent images of thick (cross-sectional area: 0.649 mm^2) and thin (cross-sectional area: 0.0262 mm^2) cardiac muscle rings (Fig. 2a). As depicted, cavities form in the central part of the tissue cross-sections,

Open Access Article. Published on 15 June 2024. Downloaded on 8/2/2025 4:02:20 PM.
This article is licensed under a Creative Commons Attribution-NonCommercial 3.0 Unported Licence.

and its size is larger as the cross-sectional area of the tissue increases. This suggests that necrosis occurred in the central part of the tissue due to inadequate oxygen permeation, leading to reduction of the contractile force per unit area. During the cultivation process of thick and thin cardiac muscle rings within the PDMS substrates, their widths decreased by approximately one-third within the initial 24 hours, attributed to the inherent self-contraction of the hydrogel. Subsequently, over the course of an additional 10 days, their widths decreased by approximately 4%, ultimately reaching values of 420 μm and 210 μm, respectively (Fig. 2b). After 11 days of culture, we removed the cardiac muscle rings from the mold and measured their contractile forces exerted by spontaneous contraction. The thick cardiac muscle rings exhibited a contractile force four times larger than the thinner ones but less than half the contractile stress (*i.e.* the contractile force per unit cross-sectional area) (Fig. 2c and d). These results indicate that while the muscular contractile force increases with the enlargement of the cross-sectional area, excessive enlargement induces necrosis, as shown in Fig. 2a. Since the force-generating units are present in areas forming muscle fibers, the decrease in contractile force per unit area occurred with larger cross-sectional areas.

Fabrication of the biohybrid self-beating actuator

To utilize the cardiac muscle rings as self-driving power sources, a biohybrid self-beating actuator was constructed by assembling the cardiac muscle rings with artificial components (Fig. 3a and Movie S2†). This actuator has the shape of a fish and features a structure in which two cardiac muscle rings sandwich the PDMS body, forming an antagonistic pair structure. We used the thick cardiac muscle rings exhibiting higher contractile force than thinner ones. We set the distance between the anchors to be 40% larger than the inner diameter of a cardiac muscle ring in its non-stretched state to maximize its contractile force. When one side of the cardiac muscle ring contracts, the substrate deformation displaces its tail to one side, followed by other cardiac muscle ring, displacing the tail in the opposite direction. Consequently, the continuous beating motion of the tail can occur across the body axis (Fig. 3b and Movie S3†). As can be seen from the overview images, the two ends of the cardiac muscle rings were securely connected to the anchors (Fig. 3c). Furthermore, to make the biohybrid self-beating actuator float on the surface of the culture medium, we adjusted its overall density to be lower than that of the culture medium and designed it to prevent its tail fin from touching the bottom of the culture dish.

Evaluation of the biohybrid self-beating actuator

Fig. 4a shows a conceptual diagram for observing the tail actuation of the biohybrid self-beating actuator. A reference point was designated at its tail tip, and the beating motion was observed by microscope (IX71N; Olympus), followed by motion analysis using a motion capture software program (VW-9000 motion analyzer; Keyence Corp.). The body axis was defined as the position where both muscles were in a relaxed state (Fig. 4b). We tracked the reference point over time to assess the beating motion of the tail fin. When the upper cardiac muscle ring in the images contracted and the lower one relaxed, we confirmed the upward movement of the tail. Subsequently, when both muscles relaxed, the tail returned to its original position, and it displaced downward when the force relationship was reversed (Fig. 4c and Movie S4†). We analyzed the displacement of the reference point and assessed the transition of beating motion with culture days. One day after construction, both upward and downward motion across the body axis was unstable. However, on day 4, the motion appeared more stable compared to day 1, and antagonistic movements occurred at the same time intervals. Furthermore, on day 7, the beating motion became faster and more stable compared to day 4 (Fig. 4d). Additionally, we confirmed that the beating amplitude on day 7 increased with culture, reaching approximately 1.3 times the initial value (Fig. 4e). Comparing the upward and downward displacements, the beating motion became more symmetrical (Fig. 4f). Specifically, the relative error between upward and downward displacement was 72.8% of the mean value on day

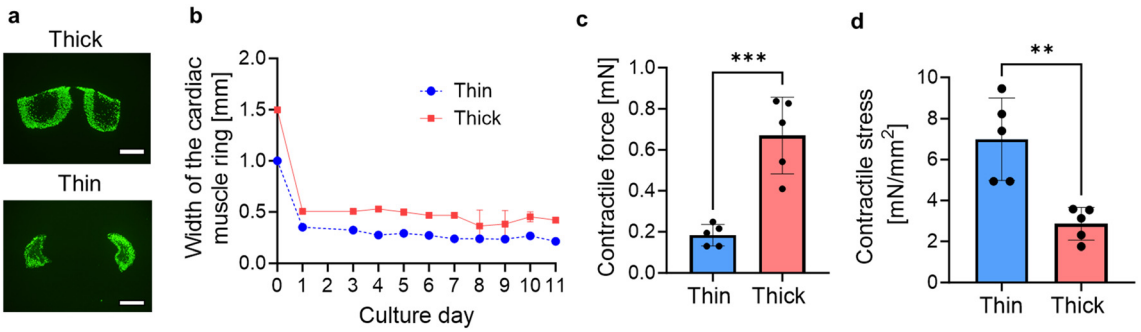

Fig. 2 Comparison of contractile forces of cardiac muscle rings (two different sizes). (a) Immunostaining images of the cross-sections of the cardiac muscle rings with different cross-sectional areas (thick: 0.23 mm^2, thin: 0.026 mm^2). (b) Width of the cardiac muscle rings with 11-days culture. Bars represent the mean ± SEM. (c) Contractile force and (d) contractile stress of the thick and thin cardiac muscle rings. Bars represent the mean ± SEM. $^{**}p < 0.005$, $^{***}p < 0.0005$, non-paired, Student's *t*-test (n = 5). Scale bars; a: 300 μm.

This journal is © The Royal Society of Chemistry 2024

Open Access Article. Published on 15 June 2024. Downloaded on 8/2/2025 4:02:20 PM.
This article is licensed under a Creative Commons Attribution-NonCommercial 3.0 Unported Licence.

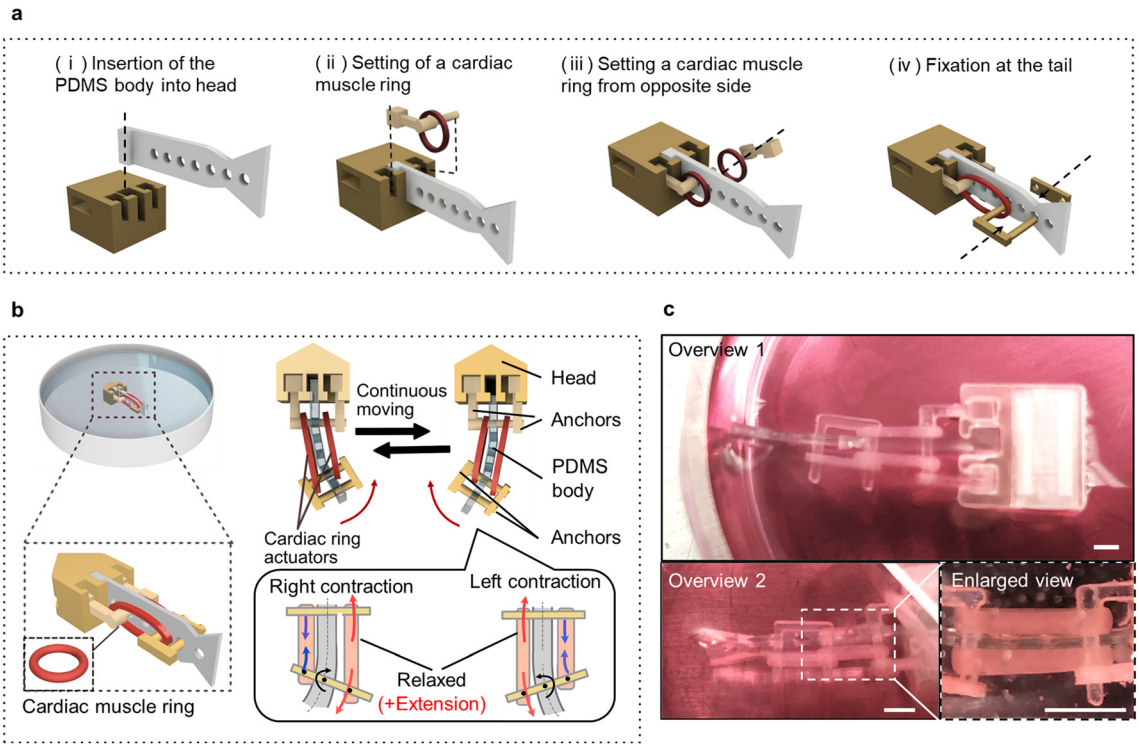

Fig. 3 Fabrication of a centimeter-sized biohybrid self-beating actuator with antagonistic pair of the cardiac muscle rings. (a) Schematic diagram of fabricating the biohybrid self-beating actuator. (b) Schematic diagram of the biohybrid self-beating actuator powered by cardiac muscle rings. The two cardiac muscle rings sandwich the PDMS body and formed an antagonistic pair structure. The beating motion at the tail portion is executed through the mutual contraction of each cardiac muscle ring. (c) Overall and enlarged views of the biohybrid self-beating actuator constructed in this study. Scale bars; 1 mm.

1, while on day 7 it reduced to 15.9%. These results suggest the following flow of events. With a mechanical coupling structure, the muscular contraction of one of the paired muscles triggers the stretching stimulus to the other paired muscle. Based on the characteristics of cardiomyocytes mentioned above, the stretched muscle reactively contracts, leading to further stretching stimuli applied to the paired cardiac muscle, and this continuous phenomenon led to the synchronized motion and the larger beating amplitude of the tail.

We measured the amplitude over 31 days to examine how the spontaneous beating motion changed during the culture period. As a result, the beating amplitude peaked on day 8, and gradually decreased to approximately by day 31 (Fig. 4g). Additionally, we also constructed the biohybrid self-beating actuator with a non-antagonistic structure and confirmed that the distance between the anchors shortened due to the lack of muscular tension balance (Fig. S3 and Movie S5†). This result demonstrates that the antagonistic pair structure allows our biohybrid self-beating actuator to continue its actuation for a longer period.

Electrical stopping of the biohybrid self-beating actuators

Although spontaneous contractions of the conventional cardiac actuators enable them to actuate without an electric power supply, it has been still a challenge to stop their motions. To stop the motions, we applied electric stimuli across the entire biohybrid self-beating actuator, allowing an electric field to penetrate both antagonistic cardiac muscle rings (Fig. 5a). Consequently, the application of an electric field resulted in a significant reduction in the tail's beating amplitude. Once the electric stimuli turned off, the tail motion returned to its original beating motion (Fig. 5b and Movie S6†). We varied the intensity of the electric field and assessed the change in the tail motion, and confirmed that electric field application resulted in an increase in beating frequency and a decrease in beating amplitude (Fig. 5c and d). These results demonstrate that the increase of the electric field can suppress the motion of the actuator.

Discussion

In this paper, we utilized 3D cardiac muscle tissues to build robotic actuators. The cardiac muscle rings exhibited spontaneous contraction at regular intervals, and we found that providing electrical stimulation increased their contractile frequency, while applying static strain enhanced their contractile force. Subsequently, we constructed the biohybrid self-beating actuator by the pick-and-place method, and we confirmed the increase and transition in tail movement from unstable to stable over time in culture. Furthermore, as with

Open Access Article. Published on 15 June 2024. Downloaded on 8/2/2025 4:02:20 PM.
This article is licensed under a Creative Commons Attribution-NonCommercial 3.0 Unported Licence.

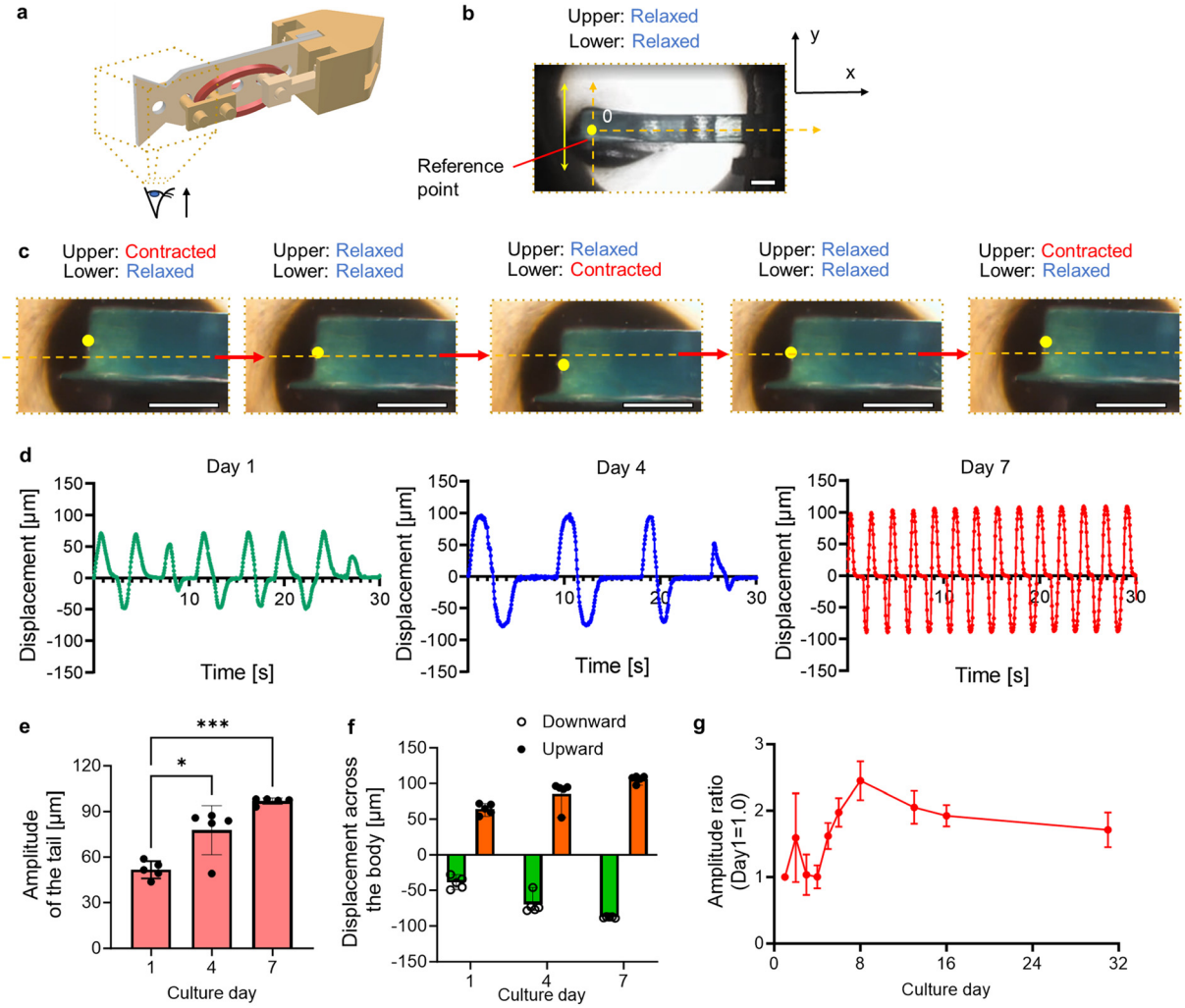

Fig. 4 Driving characteristics of the biohybrid self-beating actuator. (a) Conceptual image of observation. (b) Enlarged view of the tail fin. (c) Temporal tracking of the reference point for evaluating the tail beating motion. (d) Temporal change in displacement of the reference point. The results are illustrated on day 1, 4, and 7, respectively. (e) Beating amplitude of the tail with culture. Bars represent the mean ± SEM. $*p < 0.05$, $***p < 0.0005$, Tukey–Kramer test ($n = 4$). (f) Average upward and downward displacement across the body axis with culture. Bars represent the mean ± SEM ($n = 4$). (g) Lifetime of the biohybrid self-beating actuator with an antagonistic and a non-antagonistic pair of the cardiac muscle rings. The temporal evolution of the tail's amplitude was recorded over a period of 31 days. Bars represent the mean ± SD, $n = 3$. All scale bars: 5 mm.

the antagonistic pair structure of cardiac muscle rings, we not only sustained its spontaneous tail movement for one month but also temporarily suppressed it by applying an electric field to both antagonistic muscles.

When constructing biohybrid actuators or robots with high actuation efficiency, we need to place the driving sources within the limited 3D space. Therefore, the improvement of the contractile force per unit footprint is a crucial factor for driving sources. Our constructed cardiac muscle rings have both a width and a thickness of approximately 200–500 μm, and the circumferential length of the ring ranges from 6.2 to 12.5 mm, resulting in an estimated contractile force per unit footprint of approximately 100 to 250 μN mm^{-2}. In contrast, conventional 2D cardiac muscle tissues had a wide range of widths, but their thicknesses were limited to 4–6 μm per layer, reaching a maximum of 21–23 μm when stacking layers.[17–19] The order of estimated contractile force per unit footprint of the conventional 2D cardiac muscle tissues ranges from 0.1 to 10 μN mm^{-2}.[7–10,17–22] Therefore, we believe that cardiac muscle rings are strong and useful as driving sources when considering placement in 3D spatial configurations. Although 3D cardiac muscle tissues experience a decrease in contractile stress when their cross-sectional area becomes excessively large due to necrosis (cell death) as shown in Fig. 2c and d, these tissues are anticipated to generate greater force in appropriately narrow spaces compared to their 2D counterparts.

The targeted characteristics of cardiac muscle rings in this study include (i) the generation of muscular force through autonomously rhythmic contraction of muscle fibers, (ii) frequency responsiveness when subjected to electrical pulses, and (iii) the ability to generate sufficient contractile force to drive artificial devices (the fishtail). First, the direct transmission of force to anchors through muscle fiber contraction can

 This journal is © The Royal Society of Chemistry 2024

Open Access Article. Published on 15 June 2024. Downloaded on 8/2/2025 4:02:20 PM.
This article is licensed under a Creative Commons Attribution-NonCommercial 3.0 Unported Licence.

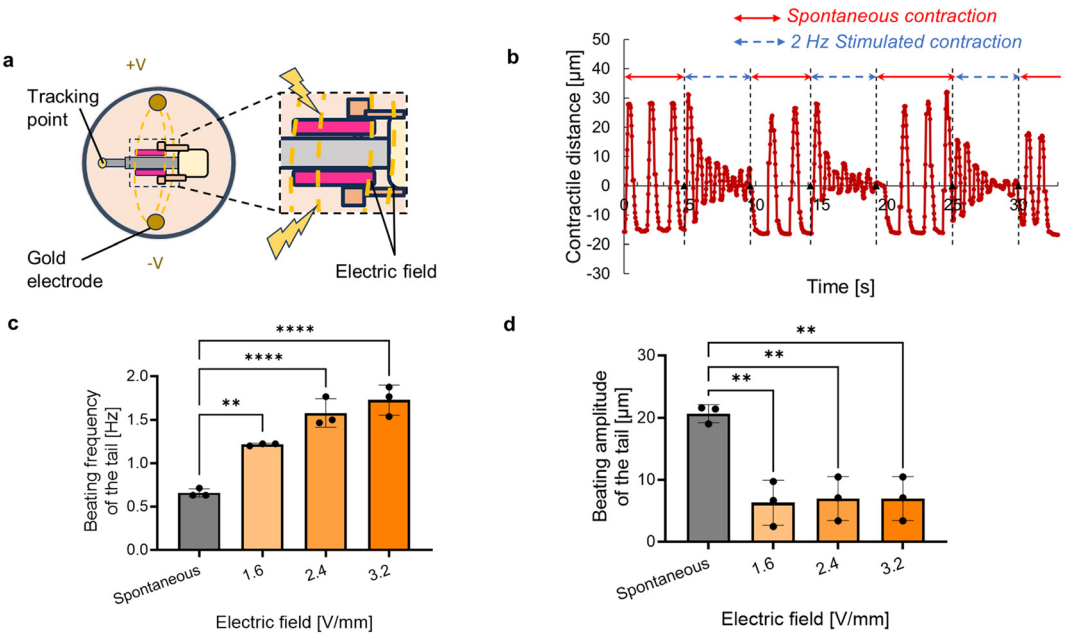

Fig. 5 Evaluation of the controllability of the biohybrid self-beating actuator. (a) Schematic diagram of the electric field application to the biohybrid self-beating actuator. (b) Temporal beating displacement of the tail when the electric field is intermittently applied. (c) Beating frequency and (d) beating amplitude of the tail when the electric field is applied. Bars represent the mean ± SEM. $^{**}p < 0.005$, $^{****}p < 0.0001$, Tukey–Kramer test (n = 3).

be verified by the changes in inner diameter during contraction and the contractile force data, which aligns with our expectations. Second, the cardiac muscle rings repeatedly contract at a speed of 2 Hz when subjected to 2 Hz electrical pulses. The result is consistent with the previous study[23] and showcases the controllability of such types of actuators. While there is still room for improving the maturity of human-induced pluripotent stem cell-derived cardiomyocytes, the current tissue can generate a maximum contractile force of up to 850 μN, which is sufficient to drive artificial devices into beating motion. These results led us to believe that our cardiac muscle rings possess adequate characteristics as robotic actuators. According to previous work[24] which utilized cardiomyocytes with differentiation efficiencies exceeding 90%, the resulting tissues – comparable to our cardiac muscle rings in size and contractility – produced force outputs that match those observed in our study. This correspondence suggests that our cardiomyocyte differentiation may also be at a comparable purity level.

In this study, it is also noteworthy that hiPSC-derived cardiac cells were used for the construction of a cardiac muscle ring. Conventional biohybrid cardiac actuators have typically utilized 2D cardiac muscle tissues from living animals such as rats or mice. These choices have been made due to limitations in cell numbers resulting from difficulties in cardiomyocyte proliferation[25] and ethical concerns associated with use as robotic actuators.[26,27] In contrast, hiPS cells are proliferative cells, and the differentiation protocols for cardiomyocytes have been extensively studied. Therefore, we obtained cardiomyocytes with 2.5×10^7 cells per sample through a differentiation process from hiPS cells. Cardiomyocytes derived from hiPS cells generally exhibit inferior contractile force per muscle fiber compared to native ones due to their biologically immature phenotype. However, when constructing 3D tissues, they offer advantages such as the ability to increase their height and facilitate easier cell numbers while minimizing ethical concerns.

As shown in Fig. 1h and i, we confirmed that the temporal application of stretching stimuli resulted in improved muscular contractile force. This phenomenon has also been reported in the organ-on-a-chip field, where it has been suggested that the stretching tension enhanced muscle fiber formation and orientation within 3D architecture, promoting tissue maturation.[28–30] Additionally, cardiomyocytes *in vitro* exhibit significant contractility with increase of the stretching stimuli, as is known from Starling's law of the heart.[15,31,32] Therefore, our experimental results, where muscular contractile force increased with applied external strain, can be attributed to this unique characteristic of cardiomyocytes.

The difficulty of prolonged use for measuring the contractile force of 3D cardiac muscle tissues in the organ-on-a-chip field has been raised due to the self-shortening of the muscle tissues.[23,24,33–35] In contrast, by adopting an antagonistic muscle structure, the balanced muscular tension of the antagonistic muscles suppressed asymmetrical contraction on one side, enabling beating motion for up to 31 days. Furthermore, we observed that even in immature cardiomyocytes derived from hiPS cells, the oriented muscle fibers and increase in contractility are recognized due to the continuous application of physical stretching stimuli. According to the previous work,[8] the planar configuration of cardiac tissues with an antagonistic muscle structure suggests that the repetition of

Open Access Article. Published on 15 June 2024. Downloaded on 8/2/2025 4:02:20 PM. This article is licensed under a Creative Commons Attribution-NonCommercial 3.0 Unported Licence.

rhythmic stretching and contraction prevents heterogeneity in myocardial repolarization and contraction, which is expected to enhance the understanding of structure–function relationships in cardiovascular physiology. Our approach, applying the antagonistic muscle structure to three-dimensional cardiac tissues, may present a biomimetic system capable of detailed analysis of these relationships within expanded myocardial cellular networks. Furthermore, in the conventional heart-on-a-chip field, the prevalent method involved directly forming cardiac muscle tissues on PDMS-made cantilevers and measuring forces by analyzing the cantilever's deformation. In contrast, our cardiac muscle rings, with their excellent integrability, allow for the direct measurement of contractile force using force sensors (Fig. S1†) and subsequent removal. Utilization of the cardiac muscle rings is highly effective, especially for pre-measurement of contractile force that requires two evenly opposing forces, as typically observed in structures like antagonistic muscles. For the heart-on-a-chip field, this can be beneficial when aiming to simultaneously evaluate multiple cardiac muscle tissues on a single chip.

The suppression of movement along the body axis with electrical stimuli is also thought to be attributed to the implementation of an antagonistic pair structure. The constructed free-standing cardiac muscle rings demonstrate an increase in contractile velocity in response to electrical frequency, as illustrated in Fig. 1f. When this frequent motion is simultaneously performed across the body axis, the rapid contraction timing occurring in both muscles prevents the tail from following its motion, leading to a significant suppression of tail beating amplitude. Additionally, we believe that a greater amount of electric field penetrating both muscles resulted in a higher tension balance leading to further reduction in the amplitude.

The self-beating actuator could be used to drive swimming biohybrid robots which do not require complex driving mechanisms and external power supply. There is still room for improving the contractile force of the cardiac muscle rings and the structural optimization of the actuator. *E.g.*, by promoting the maturation of hiPS-CMs or introducing artificial joints to the body, large tail movement could be enabled with a small muscular force. Also, the development of a technique to form neuromuscular junctions between neural tissues and cardiac muscle rings could lead to the adjustment of the contractile speed of the cardiac muscle rings through neural control and improve our understanding of cardiac functions.

Our study demonstrated that the cardiac muscle rings functioned as building blocks with high contractility and maneuverability, and the biohybrid self-beating actuator developed in this study serves as an example of actuators embodying the characteristics of cardiac muscle rings. Utilizing these characteristics, the integration with artificial components possessing specialized and optimized 3D frameworks could lead to the realization of autonomously driven actuators with enhanced functionalities. For example, our biohybrid self-beating actuator, being three-dimensionally thick and wide, may have the capability to accommodate artificial devices such as speedometers and accelerometers. By harnessing the spontaneous contractions of the cardiac rings to generate self-power and using this energy to power such artificial devices, it may be possible to create a "self-aware" biohybrid self-beating actuator.

Methods

Preparation of hiPS cell-derived cardiomyocytes

HiPS cells were purchased from Riken Cell Bank, and the differentiation medium was purchased from Nacalai-Tesque, Inc., and the differentiation process was followed by their protocol. In brief, a Matrigel-coated multiple-well plate was prepared, and hiPS cells were cultured in the culture dish with mTeSR1 plus growth medium (VERITAS) added 10 μM kinase inhibitor Y-27632 (Nacalai-Tesque, Inc.), at first density 1.0–2.0 × 10^4 cells per ml (day 0). After 20–24 hours, we exchanged the growth medium without Y-27632. On day 4, the growth medium was removed with a pipette and replaced with the differentiation medium (Nacalai-Tesque, Inc.) with 5–9 μM CHIR99021 (Nacalai-Tesque, Inc.) followed by washing with Iscove's modified Dulbecco's medium (Thermo Fisher Scientific, Inc.). The concentration of CHIR99021 is dependent on the iPS-cell types and plating density of hiPS cells. On day 6, the culture medium was replaced with a differentiation medium supplemented with 10 μM IWP-2 solution, 10 μM SB431542 and 100 nM β-estradiol (purchased from Nacalai-Tesque, Inc.). On day 8, the culture medium was replaced with a differentiation medium supplemented with 100 nM β-estradiol, and the culture medium was changed every other day. On day 15–17, cardiomyocytes beating in the well plates were observed. On day 20–21, we detached hiPSC-CMs from the well plates and used them for the following experiments.

Preparation of the PDMS mold

To construct the cardiac muscle rings, we prepared polydimethylsiloxane (PDMS) substrates with circular grooves. Initially, a resin-based mold was printed using a commercial stereolithography machine (DWS DIGITALWAX 028J, DWS). Subsequently, a chemical vapor deposition machine (Specialty Coating Systems) was employed for coating the mold with a 2 μm thick layer of parylene C. Parylene coating was applied to suppress the uncured phenomenon of PDMS elastomer caused by radicals present on the resin surface. Following, PDMS elastomer (Sylgard 184 Silicone Elastomer, Dow Corning Toray) mixed at a ratio of 10 : 1 (base/cross-linker) was poured into the parylene-coated resin mold and cured at 75 °C for 150 minutes. After removing the PDMS substrate from the resin mold, the PDMS substrate was washed with 70% ethanol, and subjected to sterilization using an ozone sterilizer (Genlantis) for 30 minutes. Then, we coated the PDMS substrate with 90% ethanol with 0.5 wt% phosphorylcholine-based (MPC) polymers (NOF Corporation) by incubation at 65 °C for 90 minutes, which serves to block

 This journal is © The Royal Society of Chemistry 2024

Open Access Article. Published on 15 June 2024. Downloaded on 8/2/2025 4:02:20 PM. This article is licensed under a Creative Commons Attribution-NonCommercial 3.0 Unported Licence.

adhesion of cells and hydrogels. The PDMS substrate was washed with PBS and filled with distilled water until submerged, then placed in a desiccator and degassed overnight. Degassing is to prevent air bubbles present in the PDMS from entering during the construction process of the cardiac muscle rings. 30 minutes before seeding the cell suspension, we coated the surface of the PDMS substrate with a 1% BSA/PBS solution; the BSA coating serves to inhibit specific adhesion of the proteins contained in 3D tissues.

Fabrication of the cardiac muscle rings

After 20–21 days of culturing hiPS-CMs, the culture medium was removed from the well plates. Afterward, a collagenase solution was added (200 μL cm^{-2}) and incubated for 1–2 hours to detach hiPS-CMs from the well plates. The collagenase solution was prepared by mixing 0.5 g of collagenase I powder (Wako Pure Chemical Industries, Ltd.) with 200 ml of PBS, 50 ml of FBS (Thermo Fisher Scientific, Inc.), and 2 ml of D-PBS (+) (Nacalai-Tesque, Inc.) and filtering it. After hiPS-CMs were detached from the well plates, cell detachment enzyme (Accumax; Nacalai-Tesque, Inc.) was added (200 μL cm^{-2}) and incubated for 15 minutes to disperse hiPS-CMs into single cells. If hiPS-CMs were not sufficiently dispersed, we gently pipetted and additionally incubated for up to 15 minutes. Subsequently, the cell suspension was filled in a 15 ml tube and centrifuged at 1 × *g* for 6 minutes. After centrifugation, the supernatant was completely removed, and hiPS-CMs were mixed with precursor gel solution. Precursor gel solution used per one cardiac muscle ring consisted of 48 μL fibrinogen (12.5 μg ml^{-1}) (Sigma-Aldrich), 6.4 μL Matrigel (Corning), 5 μM Y-27632, and 33.3 μg ml^{-1} aprotinin (Sigma-Aldrich). 9.6 μL thrombin (0.5 unit per ml) (Sigma-Aldrich) was separately prepared and mixed with other solutions just before seeding in the PDMS mold (coated by MPC polymer and BSA) because it immediately solidified upon mixing with fibrinogen. The final cell density of a cardiac muscle ring was 2.5×10^7 cells per ml. After seeding the cell-suspended solutions into the PDMS substrate, we incubated them for 10 minutes to promote gelation. Subsequently, the tissue culture medium was added until the PDMS substrates were submerged and, then we started cultivation. The tissue culture medium consisted of DMEM (high glucose) supplemented with 10% FBS, 1% penicillin–streptomycin, 33.3 μg ml^{-1} aprotinin, and 10 μM Y-27632. After incubation for 20–24 hours, the tissue culture medium without Y-27632 was replaced and was exchanged every other day. Synchronized contraction movements of the cardiac muscle rings were observed 6–8 days from starting cultivation.

Fabrication process of the biohybrid self-beating actuator

The biohybrid self-beating actuator is composed of two cardiac muscle rings, two pairs of anchors, a head part, and a PDMS body. The head part and all anchors were made from resin and were fabricated using a commercial 3D printer (AGILISTA-3200; KEYENCE). The PDMS body was fabricated by pouring PDMS elastomer into a perylene-coated resin mold and baking it. The PDMS body has multiple holes longitudinally from the head to the tail, which are used to secure the cardiac muscle rings by anchoring with any position. Additionally, one end of the PDMS body has a convex part, which can be locked with the head part. Before assembly, all artificial components without the cardiac muscle rings were washed with 70% ethanol and subjected to sterilization using an ozone sterilizer. The fabrication process of a biohybrid self-beating actuator is as follows; firstly, the PDMS body is inserted and fixed with the head part (Fig. 3a(i)). After that, one cardiac muscle ring is threaded through the anchor, and fixed with the holes of the PDMS body (Fig. 3a(ii)). Subsequently, the other cardiac muscle ring is fixed on the opposite side (Fig. 3a(iii)). Afterward, the two cardiac muscle rings are pulled by using the other anchors and fixed near the tail fin (Fig. 3a(iv)).

Immunostaining and microscopy

For immunostaining of hiPS-CMs, samples (cardiac muscle rings) were washed once with PBS, fixed with 4% paraformaldehyde (PFA) (Muto Pure Chemicals Co., Ltd.) for 30 min, permeabilized cell membranes with 0.2% Triton X-100 for 15 min, and blocked with 1.0% bovine serum albumin (BSA) (Sigma-Aldrich) overnight. For actin staining, we used 0.2% Alexa Fluor 488-conjugated phalloidin (Thermo Fisher Scientific, Inc.) and incubated at room temperature for 2 hours. For α-actinin staining, we incubated samples with 0.1% monoclonal anti-α-actinin antibody (Sigma-Aldrich) as the primary antibody overnight at 4 °C, then with 0.1% goat anti-mouse IgG antibody (Thermo Fisher Scientific, Inc.) as the secondary antibody for 100 min at room temperature. Afterward, the samples were rinsed twice with PBS and incubated with 0.1% Hoechst 33342 (Invitrogen) at room temperature for 8 min to stain cell nuclei, following rinsed with PBS three times. We used a microscope (IX71N; Olympus) for bright-field and fluorescence microscopy, and a laser microscope (LSM780; Zeiss) for confocal microscopy.

Statistical analysis

Student's *t*-test or Tukey–Kramer tests were performed using the statistical software GraphPad Prism10 (**https://www.mdf-soft.com/products/prism10.html**). All data were shown as the mean ± SD or mean ± SEM.

Author contributions

Tomohiro Morita: outline generation – original draft, table and figure generation, data curation, formal analysis. Minghao Nie: supervision, editing, methodology. Shoji Takeuchi: funding acquisition, supervision, project administration, editing, resources, visualization, writing – review and editing.

Open Access Article. Published on 15 June 2024. Downloaded on 8/2/2025 4:02:20 PM. This article is licensed under a Creative Commons Attribution-NonCommercial 3.0 Unported Licence.

Conflicts of interest

There are no conflicts to declare.

References

1 L. Sun, Y. Yu, Z. Chen, F. Bian, F. Ye and L. Sun, *et al.*, Biohybrid robotics with living cell actuation, *Chem. Soc. Rev.*, 2020, **49**(12), 4043–4069, DOI: **10.1039/d0cs00120a**.

2 O. Aydin, A. P. Passaro, R. Raman, S. E. Spellicy, R. P. Weinberg and R. D. Kamm, *et al.*, Principles for the design of multicellular engineered living systems, *APL Bioeng.*, 2022, **6**(1), 010903, DOI: **10.1063/5.0076635**.

3 A. W. Feinberg, A. Feigel, S. S. Shevkoplyas, S. Sheehy, G. M. Whitesides and K. K. Parker, Muscular thin films for building actuators and powering devices, *Science*, 2007, **317**(5843), 1366–1370, DOI: **10.1126/science.1146885**.

4 S.-J. Park, M. Gazzola, K. S. Park, S. Park, V. Di Santo and E. L. Blevins, *et al.*, Phototactic guidance of a tissue-engineered soft-robotic ray, *Science*, 2016, **353**(6295), 158–162, DOI: **10.1126/science.aaf4292**.

5 H. Tetsuka, L. Pirrami, T. Wang, D. Demarchi and S. R. Shin, Wirelessly Powered 3D Printed Hierarchical Biohybrid Robots with Multiscale Mechanical Properties, *Adv. Funct. Mater.*, 2022, **32**(31), DOI: **10.1002/adfm.202202674**.

6 J. Kim, J. Park, S. Yang, J. Baek, B. Kim and S. H. Lee, *et al.*, Establishment of a fabrication method for a long-term actuated hybrid cell robot, *Lab Chip*, 2007, **7**(11), 1504–1508, DOI: **10.1039/b705367c**.

7 J. Xi, J. J. Schmidt and C. D. Montemagno, Self-assembled microdevices driven by muscle, *Nat. Mater.*, 2005, **4**(2), 180–184, DOI: **10.1038/nmat1308**.

8 K. Y. Lee, S.-J. Park, D. G. Matthews, S. L. Kim, C. A. Marquez and J. F. Zimmerman, *et al.*, An autonomously swimming biohybrid fish designed with human cardiac biophysics, *Science*, 2022, **375**(6581), 639–647, DOI: **10.1126/science.abh0474**.

9 V. Chan, K. Park, M. B. Collens, H. Kong, T. A. Saif and R. Bashir, Development of miniaturized walking biological machines, *Sci. Rep.*, 2012, **2**, 857, DOI: **10.1038/srep00857**.

10 L. Wang, W. Dou, M. Malhi, M. Zhu, H. Liu and J. Plakhotnik, *et al.*, Microdevice platform for continuous measurement of contractility, beating rate, and beating rhythm of human-induced pluripotent stem cell-cardiomyocytes inside a controlled incubator environment, *ACS Appl. Mater. Interfaces*, 2018, **10**(25), 21173–21183, DOI: **10.1021/acsami.8b05407**.

11 J. Y. Kim, Y.-S. Choi, B.-K. Lee and D.-W. Lee, Surface-patterned SU-8 cantilever arrays for preliminary screening of cardiac toxicity, *Biosens. Bioelectron.*, 2016, **80**, 456–462, DOI: **10.1016/j.bios.2016.01.089**.

12 C. Williams, A. W. Xie, M. Yamato, T. Okano and J. Y. Wong, Stacking of aligned cell sheets for layer-by-layer control of complex tissue structure, *Biomaterials*, 2011, **32**(24), 5625–5632, DOI: **10.1016/j.biomaterials.2011.04.050**.

13 B. C. Isenberg, D. E. Backman, M. E. Kinahan, R. Jesudason, B. Suki and P. J. Stone, *et al.*, Micropatterned cell sheets with defined cell and extracellular matrix orientation exhibit anisotropic mechanical properties, *J. Biomech.*, 2012, **45**(5), 756–761, DOI: **10.1016/j.jbiomech.2011.11.015**.

14 M. D. Lemoine, T. Krause, J. T. Koivumäki, M. Prondzynski, M. L. Schulze and E. Girdauskas, *et al.*, Human Induced Pluripotent Stem Cell–Derived Engineered Heart Tissue as a Sensitive Test System for QT Prolongation and Arrhythmic Triggers, *Circ.: Arrhythmia Electrophysiol.*, 2018, **11**(7), e006035, DOI: **10.1161/CIRCEP.117.006035**.

15 J. P. Konhilas, T. C. Irving and P. P. de Tombe, Frank-Starling law of the heart and the cellular mechanisms of length-dependent activation, *Pfluegers Arch.*, 2002, **445**(3), 305–310, DOI: **10.1007/s00424-002-0902-1**.

16 S. Schaaf, A. Shibamiya, M. Mewe, A. Eder, A. Stöhr and M. N. Hirt, *et al.*, Human engineered heart tissue as a versatile tool in basic research and preclinical toxicology, *PLoS One*, 2011, **6**(10), e26397, DOI: **10.1371/journal.pone.0026397**.

17 K. Sakaguchi, H. Takahashi, Y. Tobe, D. Sasaki, K. Matsuura and K. Iwasaki, *et al.*, Measuring the Contractile Force of Multilayered Human Cardiac Cell Sheets, *Tissue Eng., Part C*, 2020, **26**(9), 485–492, DOI: **10.1089/ten.TEC.2020.0164**.

18 V. Serpooshan, P. Chen, H. Wu, S. Lee, A. Sharma and D. A. Hu, *et al.*, Bioacoustic-enabled patterning of human iPSC-derived cardiomyocytes into 3D cardiac tissue, *Biomaterials*, 2017, **131**, 47–57, DOI: **10.1016/j.biomaterials.2017.03.037**.

19 D. Rogozhnikov, P. J. O'Brien, S. Elahipanah and M. N. Yousaf, Scaffold Free Bio-orthogonal Assembly of 3-Dimensional Cardiac Tissue via Cell Surface Engineering, *Sci. Rep.*, 2016, **6**, 39806, DOI: **10.1038/srep39806**.

20 T. Ohya, H. Ohtomo, T. Kikuchi, D. Sasaki, Y. Kawamura and K. Matsuura, *et al.*, Simultaneous measurement of contractile force and field potential of dynamically beating human iPS cell-derived cardiac cell sheet-tissue with flexible electronics, *Lab Chip*, 2021, **21**(20), 3899–3909, DOI: **10.1039/d1lc00411e**.

21 A. W. Feinberg, P. W. Alford, H. Jin, C. M. Ripplinger, A. A. Werdich and S. P. Sheehy, *et al.*, Controlling the contractile strength of engineered cardiac muscle by hierarchal tissue architecture, *Biomaterials*, 2012, **33**(23), 5732–5741, DOI: **10.1016/j.biomaterials.2012.04.043**.

22 J. C. Nawroth, H. Lee, A. W. Feinberg, C. M. Ripplinger, M. L. McCain and A. Grosberg, *et al.*, A tissue-engineered jellyfish with biomimetic propulsion, *Nat. Biotechnol.*, 2012, **30**(8), 792–797, DOI: **10.1038/nbt.2269**.

23 Y. Morimoto, S. Mori, F. Sakai and S. Takeuchi, Human induced pluripotent stem cell-derived fiber-shaped cardiac tissue on a chip, *Lab Chip*, 2016, **16**(12), 2295–2301, DOI: **10.1039/c6lc00422a**.

24 A. Leonard, A. Bertero, J. Powers, K. M. Beussman, S. Bhandari and M. Regnier, *et al.*, Afterload promotes maturation of human induced pluripotent stem cell derived cardiomyocytes in engineered heart tissues, *J. Mol. Cell. Cardiol.*, 2018, **118**, 147–158, Available from: **https://www.sciencedirect.com/science/article/pii/S0022282818300889**.

25 S. E. Senyo, R. T. Lee and B. Kühn, Cardiac regeneration based on mechanisms of cardiomyocyte proliferation and

 This journal is © The Royal Society of Chemistry 2024

Open Access Article. Published on 15 June 2024. Downloaded on 8/2/2025 4:02:20 PM.
This article is licensed under a Creative Commons Attribution-NonCommercial 3.0 Unported Licence.

differentiation, *Stem Cell Res.*, 2014, **13**(3 Pt B), 532–541, DOI: **10.1016/j.scr.2014.09.003**.

26 V. A. Webster-Wood, M. Guix, N. W. Xu, B. Behkam, H. Sato and D. Sarkar, *et al.*, Biohybrid Robots: Recent progress, challenges, and perspectives, *Bioinspiration Biomimetics*, 2022, **18**(1), DOI: **10.1088/1748-3190/ac9c3b/meta**.

27 P. Won, S. H. Ko, C. Majidi, A. W. Feinberg and V. A. Webster-Wood, Biohybrid Actuators for Soft Robotics: Challenges in Scaling Up, *Actuators*, 2020, **9**(4), 96, Available from: **https://www.mdpi.com/2076-0825/9/4/96**.

28 E. Y. Wang, N. Rafatian, Y. Zhao, A. Lee, B. F. L. Lai and R. X. Lu, *et al.*, Biowire model of interstitial and focal cardiac fibrosis, *ACS Cent. Sci.*, 2019, **5**(7), 1146–1158, DOI: **10.1021/acscentsci.9b00052**.

29 A. Salameh, A. Wustmann, S. Karl, K. Blanke, D. Apel and D. Rojas-Gomez, *et al.*, Cyclic mechanical stretch induces cardiomyocyte orientation and polarization of the gap junction protein connexin43, *Circ. Res.*, 2010, **106**(10), 1592–1602, DOI: **10.1161/CIRCRESAHA.109.214429**.

30 K. Lu, T. Seidel, X. Cao-Ehlker, T. Dorn, A. M. N. Batcha and C. M. Schneider, *et al.*, Progressive stretch enhances growth and maturation of 3D stem-cell-derived myocardium, *Theranostics*, 2021, **11**(13), 6138–6153, DOI: **10.7150/thno.54999**.

31 A. V. Delicce and A. N. Makaryus, *Physiology, frank starling law*, **europepmc.org**, 2017, [cited 2024 Jan 3], Available from: **https://europepmc.org/books/nbk470295**.

32 V. Sequeira and J. van der Velden, Historical perspective on heart function: the Frank–Starling Law, *Biophys. Rev.*, 2015, **7**(4), 421–447, DOI: **10.1007/s12551-015-0184-4**.

33 J. T. Hinson, A. Chopra, N. Nafissi, W. J. Polacheck, C. C. Benson and S. Swist, *et al.*, HEART DISEASE. Titin mutations in iPS cells define sarcomere insufficiency as a cause of dilated cardiomyopathy, *Science*, 2015, **349**(6251), 982–986, DOI: **10.1126/science.aaa5458**.

34 K. Ronaldson-Bouchard, S. P. Ma, K. Yeager, T. Chen, L. Song and D. Sirabella, *et al.*, Author Correction: Advanced maturation of human cardiac tissue grown from pluripotent stem cells, *Nature*, 2019, **572**(7769), E16–E17, DOI: **10.1038/s41586-019-1415-9**.

35 H. Li, S. Sundaram, R. Hu, L. Lou, F. Sanchez and W. McDonald, *et al.*, Dynamic Control of Contractile Force in Engineered Heart Tissue, *IEEE Trans. Biomed. Eng.*, 2023, **70**(7), 2237–2245, DOI: **10.1109/TBME.2023.3239594**.